

Janus Microdimer Surface Walkers Propelled by Oscillating Magnetic Fields

Tianlong Li, Anning Zhang, Guangbin Shao, Mengshi Wei, Bin Guo, Guangyu Zhang,* Longqiu Li,* and Wei Wang*

Recent strides in micro- and nanofabrication technologies have enabled researchers to design and develop micro- and nanoscale robotic systems with enhanced power, functionality, and versatility. Because of their capability of remote actuation and navigation, synthetic micro- and nanomotors powered by oscillating magnetic fields have recently gained considerable attention. In this article, a new type of magnetic surface walker that can achieve speeds of up to $18.6 \mu\text{m s}^{-1}$ (≈ 4 body length s^{-1}) in an oscillating magnetic field operated at 25 Hz and ≈ 2.7 mT is reported. Two magnetic Janus microspheres spontaneously form a microdimer via magnetic dipolar interactions, and this microdimer rolls its two “feet” back and forth in an alternating fashion. In addition to propulsion, the oscillating magnetic field can also precisely steer these surface walkers through complicated structures, and an extensive discussion of their performance in various experimental conditions is provided. The reported propulsion mechanism opens new possibilities for the design of remotely actuated microrobots for a wide range of applications.

1. Introduction

Powering synthetic micro- and nanoswimmers in a low Reynolds number regime is an exciting yet challenging task fueled by popular fantasies and engineering ambitions.^[1–9] Recent strides in micro- and nanofabrication technologies have sparked the development of functional micromachines with enhanced power and versatility.^[10–15] These “micromotors”, as they are commonly called, convert various types of energy into mechanical motion while overcoming viscous drag forces and thermal fluctuations. Preliminary yet exciting applications of micromotors have emerged in the fields of drug delivery,^[16–19] biosensing,^[20,21] environmental remediation,^[22–24] active material

assembly,^[25–28] nanoscale lithography, and super-resolution optical imaging.^[29,30] Among the many developed methods for powering these micromotors, magnetic fields have been popular because they can be applied remotely and noninvasively and objects can be simultaneously steered and powered.^[6–9]

Magnetically powered micromotors can be further categorized into two groups based on how the magnetic field is applied. The motors in the first group, inspired by bacterial flagella, rotate their helix-shaped bodies in a rotating magnetic field and move along their long axes like a screw.^[31–39] Those in the second group move in oscillating magnetic fields and rely on asymmetrical shape deformation to escape the constraints of the scallop theorem (i.e., purely reciprocal motion does not

lead to net displacement in low Reynolds number media).^[40–44] Dreyfus et al.^[40] developed the first micromotor driven by an oscillating magnetic field by attaching a linear chain of colloidal magnetic particles to a red blood cell. More recently, the Nelson and Wang groups independently demonstrated the undulatory locomotion of multilink magnetic nanoswimmers.^[42–44]

Both mechanisms and their respective experimental implementations require a nonreciprocal change in the particle configuration, be it the screw-like rotation of helical bodies or the undulatory motion of flexible chains, and are, in principle, insensitive to whether the particles move in the bulk or near boundaries. This insensitivity to location is very different from that of another type of magnetically powered micromotors, called “surface walkers”, which only move near a surface. For example, recent studies have shown that, when actuated by a rotating magnetic field and placed near a surface, magnetic dimers,^[45] Janus or uniform microspheres,^[46,47] clusters,^[48] colloidal chains,^[49] nanowires,^[50] and microcages^[51] can all start rolling in a directional motion, while their reciprocal dynamics in the bulk would result in no net displacement. One of the limitations of the above studies, however, is the use of a rotating magnetic field, which requires slightly sophisticated Helmholtz coil setups.

The study of micromotor dynamics near boundaries or in close confinement is of great importance and has seen a tremendous growth in academic interest.^[52–55] These studies are important not only because many of the proposed applications involving micromotors occur in confined geometries, such as blood vessels, microfluidic chips, or other liquid–solid or liquid–air

Dr. T. Li, G. Shao, Prof. B. Guo, Prof. G. Zhang, Prof. L. Li
Key Lab for Microsystems and Microstructure Manufacturing
Harbin Institute of Technology
Harbin, Heilongjiang 150001, China
E-mail: zgyqx@hit.edu.cn; longqiu@hit.edu.cn

Dr. T. Li, G. Shao, Prof. G. Zhang, Prof. L. Li
State Key Laboratory of Robotics and System
Harbin Institute of Technology
Harbin, Heilongjiang 150001, China

A. Zhang, M. Wei, Prof. W. Wang
School of Materials Science and Engineering
Harbin Institute of Technology (Shenzhen)
Shenzhen, Guangdong 518055, China
E-mail: weiwangsz@hit.edu.cn

DOI: 10.1002/adfm.201706066

interfaces, but also because they shed light on how living microorganisms and cells move in similar environments. In this spirit and with the goal of developing an alternative strategy for powering magnetic micromotors in a simpler configuration, we herein report the propulsion and steering of magnetic microdimers in an oscillating magnetic field. This new microdimer surface walker consists of two Ni/SiO₂ (or polystyrene) Janus microspheres connected by magnetic forces. Remarkably, in response to a planar oscillating magnetic field, the two hinged spheres move back and forth asymmetrically, leading to a net displacement of the microdimer. A maximum speed of 18.6 μm s⁻¹ (≈4 body length s⁻¹) was recorded for the reported micromotor at a driving frequency of 25 Hz and a magnetic field strength of 2.7 mT. Fast and accurate magnetic steering of these micromotors in complex environments and near obstacles were also demonstrated. This fuel-free micromotor represents the latest effort toward the development of fast, efficient, and controllable micro-devices that are promising for a number of potential applications.

2. Results and Discussion

The experimental setup and sample fabrication of our experiments are represented in **Figure 1**. Janus microspheres were fabricated by half-coating silica (SiO₂) microspheres 3 μm in

diameter with a 15 nm thick layer of nickel (Ni) by electron beam evaporation (Figure 1B). We note that the Janus particles made of polystyrene microspheres showed the same qualitative behaviors. The surface morphology of these Ni-SiO₂ spheres was confirmed with optical microscopy and scanning electron microscopy (SEM) (Figure 1D). When exposed to an external magnetic field generated by an electromagnetic coil placed to one side of the sample stage (Figure 1A), the ferromagnetic Ni layer on the SiO₂-Ni Janus sphere became magnetically polarized. Due to magnetic dipole-dipole interactions, two such Janus spheres were attracted to each other and formed a dimer with a staggered shape (Figure 1C,D). The Ni patches where two spheres bind serve as a hinge that enables periodic rolling under an external oscillating magnetic field, which will be discussed in more detail later.

Not only does the oscillating magnetic field induce dipole-dipole interactions between two Janus spheres, it also propels the forward motion of the formed dimer (Video S1, Supporting Information). Sinusoidal waves were generated by a waveform generator and amplified before being applied to an electromagnetic inductor, which generated an oscillating magnetic field. In such a field with an appropriate driving frequency and amplitude (discussed later), the microdimers first aligned their long axes (the line connecting the sphere centers) to the field direction at an angle of 47.6 ± 2.6° (**Figure 2A,B**) and then began

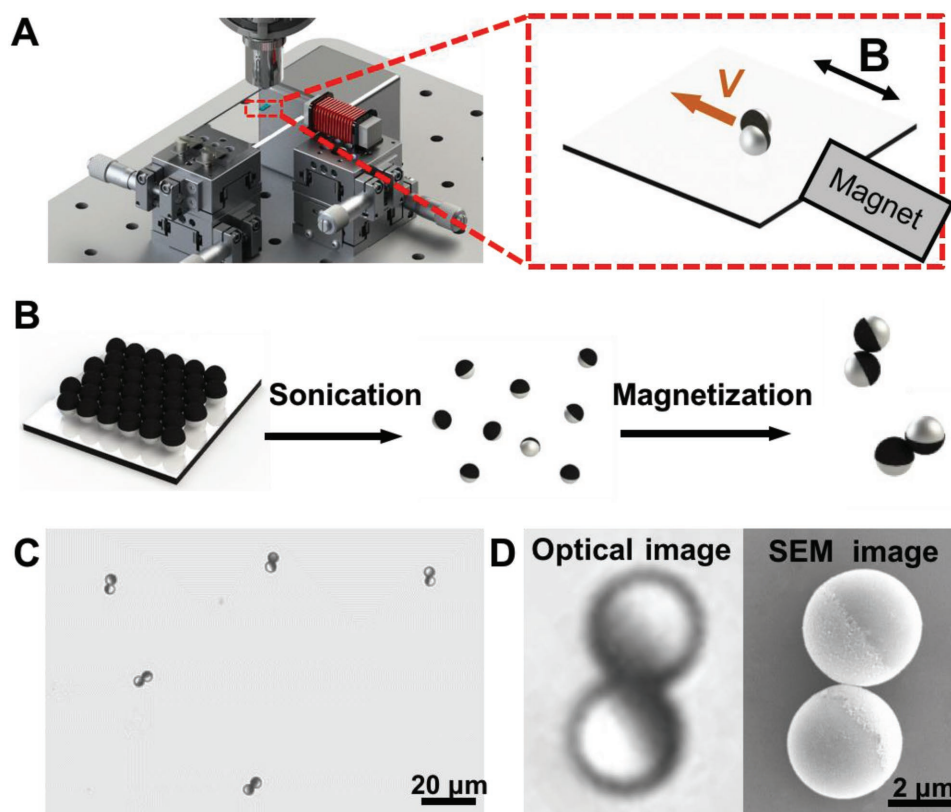


Figure 1. Design and fabrication of microdimer surface walkers. A) Schematic of the experimental setup in which a magnetic dimer moves along the magnetic field direction and away from the magnet. B) Fabrication of the microdimers. Ni-SiO₂ magnetic Janus microspheres were fabricated by coating a monolayer of silica microspheres with a thin layer of Ni, and they bind to form dimers when exposed to a magnetic field. C) Optical microscopy image of a few representative microdimers after magnetization. D) Magnified optical microscopy image and the corresponding SEM image of a microdimer, highlighting its staggered shape and the magnetic hemispheres (dark under the optical microscope and bright under the SEM).

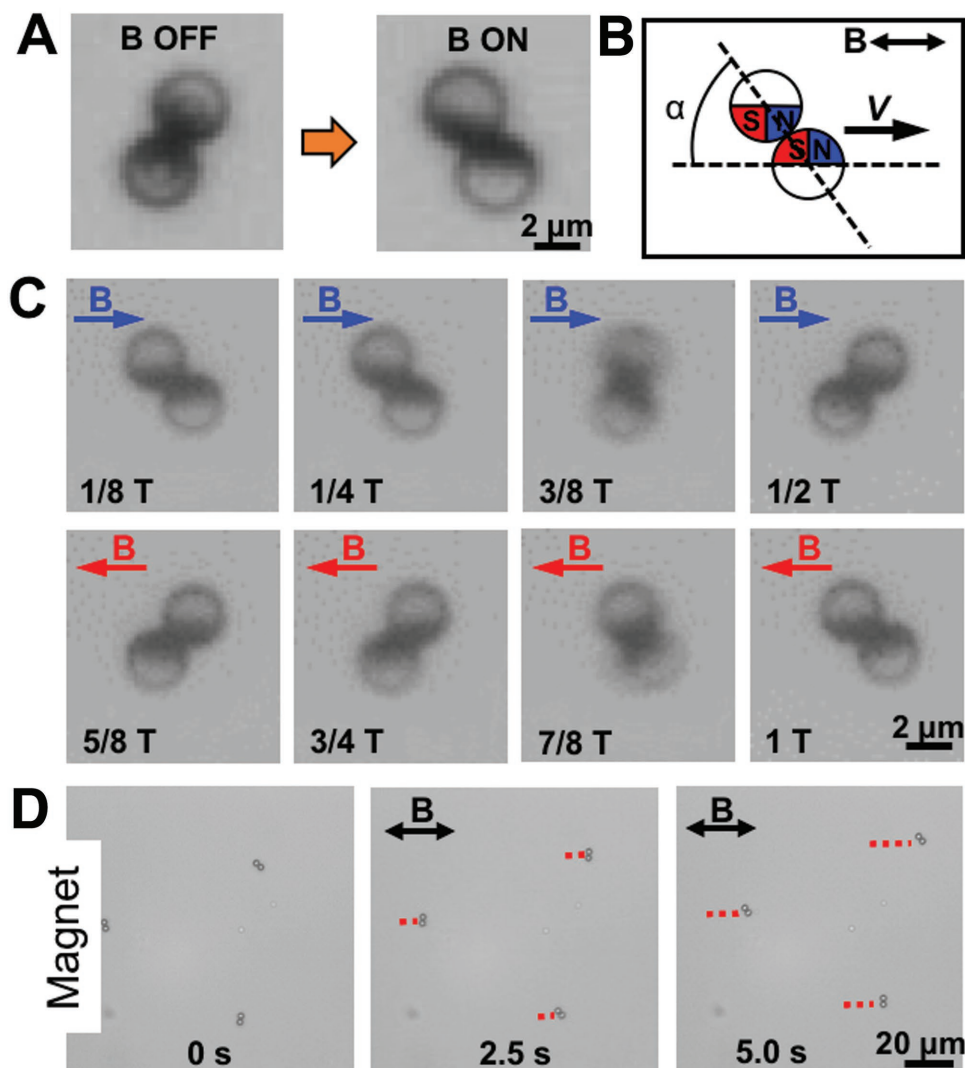


Figure 2. Propulsion of microdimer surface walkers under an oscillating magnetic field. A,B) When exposed to a magnetic field, the dimer immediately aligns its major axis with the field direction at an angle α of $47.6 \pm 2.6^\circ$, determined by the dimer geometry. C) Time-lapse optical microscopy images depicting the alternation of the two “feet” of a microdimer in an oscillating magnetic field. D) Trajectories of three representative microdimer surface walkers over 5 s. The relative position of the magnet is marked to indicate that the dimers moved away from the magnet.

to move in the direction of decreasing magnetic field strength (i.e., away from the magnet). This staggered geometry is a natural consequence of two magnetic spheres trying to minimize their magnetic energies and is consistent with previous studies, where similar dipolar interactions occurred in either AC magnetic or electric fields^[56–58] or even in chemical gradients.^[59–61] Upon closer examination, the microdimer did not move by simply sliding its body forward but rather by alternating its two spheres back and forth. A series of time-lapse snapshots shown in Figure 2C captures this process in more detail: during half of the sinusoidal cycle, one of the two spheres in the dimer rolled upward (out of the plane) and then forward, while the other sphere slid backward; during the next half of the cycle, the two spheres switched roles, and the trailing sphere rolled forward to become the leading one. The rolling of the two spheres was then repeated in subsequent cycles, propelling the dimer forward. Figure 2D shows the continuous motion of three

microdimers over 5 s at a speed of $10.6 \mu\text{m s}^{-1}$ (≈ 2 body length s^{-1}) and a driving frequency of 12 Hz.

Such a rolling motion is likely a response of the magnetically polarized microspheres to a weak oscillatory magnetic field, and we propose the following qualitative mechanism (illustrated in Figure 3A,B). First, previous studies have measured the in-plane coercivity field of 18 nm thick Ni to be ≈ 3 mT,^[62] and a series of measurements by Choi et al. showed a coercivity of ≈ 2 –3 mT for Ni films ≈ 20 nm thick.^[63] Since relatively weak magnetic fields were applied in our experiments (≈ 1 mT, see Figure S1, Supporting Information), the strength of the field in the reverse direction was not sufficient to reach the coercivity required to demagnetize the Ni layer or to switch its magnetic polarity. Therefore, to minimize the magnetic energy, a magnetic torque acted on both spheres, whose magnetic dipoles still pointed in the original direction; thus, the spheres rolled 180° to comply with the newly established magnetic field direction.

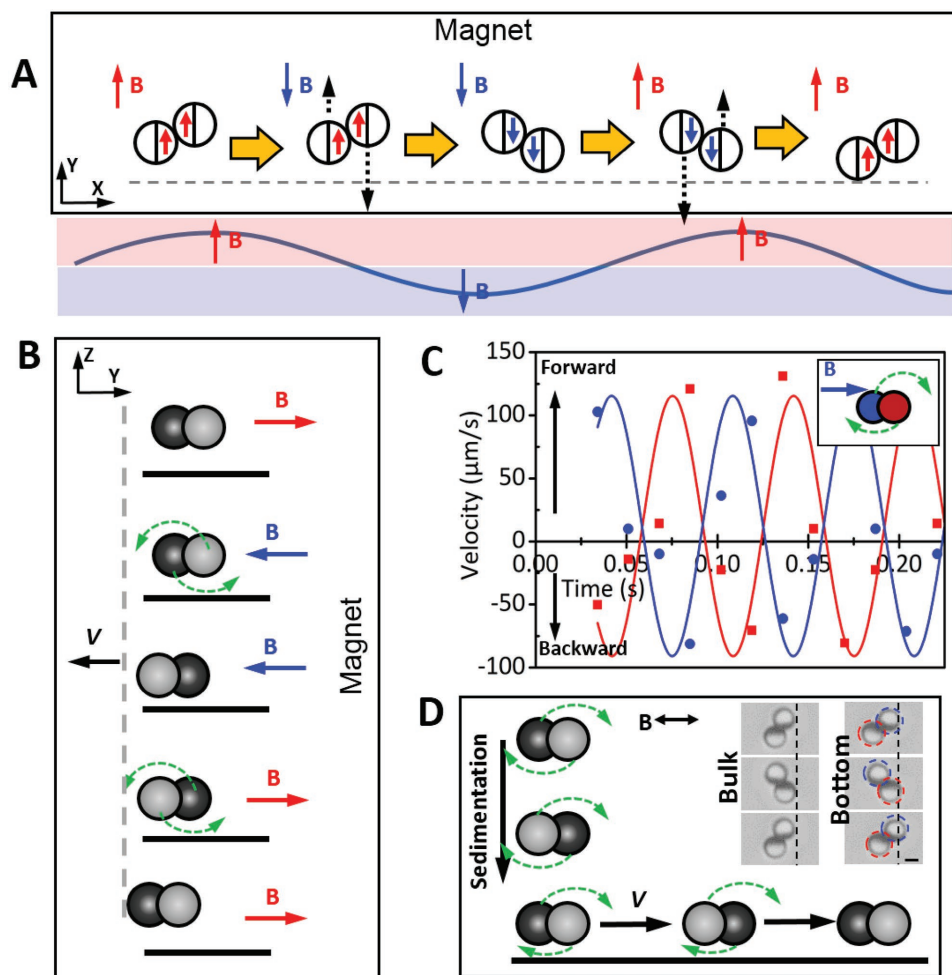


Figure 3. Propulsion mechanism of microdimer surface walkers under an oscillating magnetic field. Schematics showing the A) top and B) side views of the rolling motion of a microdimer. The red and blue arrows on the dimer indicate the magnetic polarization of the Ni hemispheres. C) Instantaneous velocity of both spheres (color coded by the inset cartoon) in a moving microdimer over 0.225 s, with positive and negative values corresponding to forward and backward rolling, respectively. Solid lines are sinusoidal fits. For each sphere (color), the area in the positive region is larger than that in the negative region, indicating a net displacement of the microdimer in the forward direction. D) Motion of a microdimer in the bulk versus when settled near a surface. Inset: optical microscopy images showing how a levitated microdimer oscillates with no net displacement, while the one near the bottom moves forward (to the right) after one cycle of rolling. Scale bar: 2 μm .

Because the two spheres in the dimer were strongly bound via Ni patches, they did not roll independently but rather in a coordinated and hinged fashion.

How does the symmetric oscillation of the driving field result in asymmetric and directional microdimer motion? After all, the “scallop theorem” proposed by Purcell famously predicted that reciprocal motion, such as rolling forward and backward in an oscillating magnetic field, would not lead to net motion for microswimmers operating at a low Reynolds number. The presence of a boundary is critical for overcoming this theorem to make “surface walkers” feasible. Specifically, although a sphere in a dimer can freely roll forward from the top, the backward roll of the sphere underneath is hindered by the limited space and presumably higher drag force (Figure 3B). Consequently, during one cycle, the forward-rolling sphere carries the dimer forward for a longer distance than the backward-rolling one, leading to a net forward motion. This mechanism of motion is supported by the data shown in Figure 3C, in which each of the two

spheres of a dimer moving at 15 Hz was individually tracked. The speeds of the spheres oscillate in synchronization with the phases of the applied magnetic field and thus fit to a sine function. The tracking results reveal that during one full cycle, a sphere traveled an average of 2.52 μm while rolling forward and only 1.70 μm when rolling backward. This discrepancy leads to a net displacement of 0.82 $\mu\text{m cycle}^{-1}$ and a speed of 12.2 $\mu\text{m s}^{-1}$, which agrees well with the dimer speed calculated by manually tracking the dimer as a whole (12.5 $\mu\text{m s}^{-1}$). Finally, a field gradient is likely necessary for a dimer to continuously move in one direction. Since at each half cycle the field and magnetic dipoles are always opposite, the overall interaction between a dimer and the magnetic field is repulsive. Even though a quick calculation shows that the two spheres experience a difference in the magnetic field strength of only 7×10^{-3} mT, or 1%, minimization of the magnetic energy still dictates that the dimer moves away from the magnet. We acknowledge that even though this proposed mechanism could qualitatively

explain why a dimer rolled in an oscillating magnetic field and why away from the magnet, a more comprehensive and quantitative study is needed and under way.

The importance of the boundary is perhaps best demonstrated by its absence (Figure 3D, Video S2, Supporting Information); thus, we designed experiments in which the Janus particles were lifted far away from any boundaries via an acoustic levitation technique.^[28] In the bulk, the dimers formed when exposed to an oscillating magnetic field in the same way as near a substrate, but the formed dimers only rolled back and forth at the same spot without any net motion, consistent with the scallop theorem. Once the dimer settled to the bottom, it immediately began to move forward. This is the most direct evidence that these magnetic microdimers break the symmetry by coupling their oscillation to a boundary.

Having explored the propulsion mechanism of the microdimers in an oscillating magnetic field, we then turned our attention to their performance under various conditions, which is critical for many of the proposed applications of micromachines. A total of four variable parameters were examined: the driving frequency, sphere size, driving voltage (i.e., the magnetic field strength), and waveform of the magnetic field. First, **Figure 4A** compares the 5 s trajectories of the 3 μm microdimer surface walkers at oscillating magnetic field frequencies from 5 to 45 Hz. This comparison is quantitatively presented in **Figure 4B**, and the motors moved at a peak speed of $15.9 \mu\text{m s}^{-1}$ at a frequency of 20 Hz, beyond which the motor speed decreased (Video S3, Supporting Information). Such a step-out frequency is commonly observed for many types of micromotors powered by oscillating magnetic fields.^[42,44] Here, we

suspect that the maximum available magnetic torque is insufficient for overcoming the fluidic drag, leading to deceleration as the microdimer surface walker moves out-of-sync with the applied magnetic field.^[34,42,44] Second, Janus spheres with three diameters (2.5, 3, and 5 μm) were fabricated, and their corresponding microdimers were tested in oscillating magnetic fields (**Figure 4B**). The step-out frequencies of the larger microdimers were found to be lower than those of the smaller dimers under similar driving conditions. Furthermore, **Figure 4C** displays the velocities of the microdimer surface walkers operated with driving voltages ranging from 50 to 200 mV (corresponding to a magnetic field strength of 1.4–5.6 mT). The speed of the microdimer surface walker under each oscillating frequency increases with increasing input voltage of the magnetic field. Finally, we investigated the effect of the oscillating magnetic field waveform on the speed of the microdimer surface walker. As shown in **Figure 4D**, varying the waveform (square wave, triangle wave, and sine wave) had minimal effect on the performance of the microdimer surface walkers.

For biomedical applications that require operation in biological fluids, tests of the propulsion performance of microdimer surface walkers in liquid media with different viscosities and salt concentrations are critical. The solution viscosity was varied by changing the concentration of glycerol in water from 0% (viscosity of 1.21 cP) to 40% (viscosity of 4.32 cP). Our experimental results, shown in **Figure 5A,B**, demonstrate that the motion of our microdimer surface walkers slowed significantly in highly viscous media. This was expected since the viscous drag at low Reynolds number is known to scale with viscosity, and our data qualitatively agree with this trend.

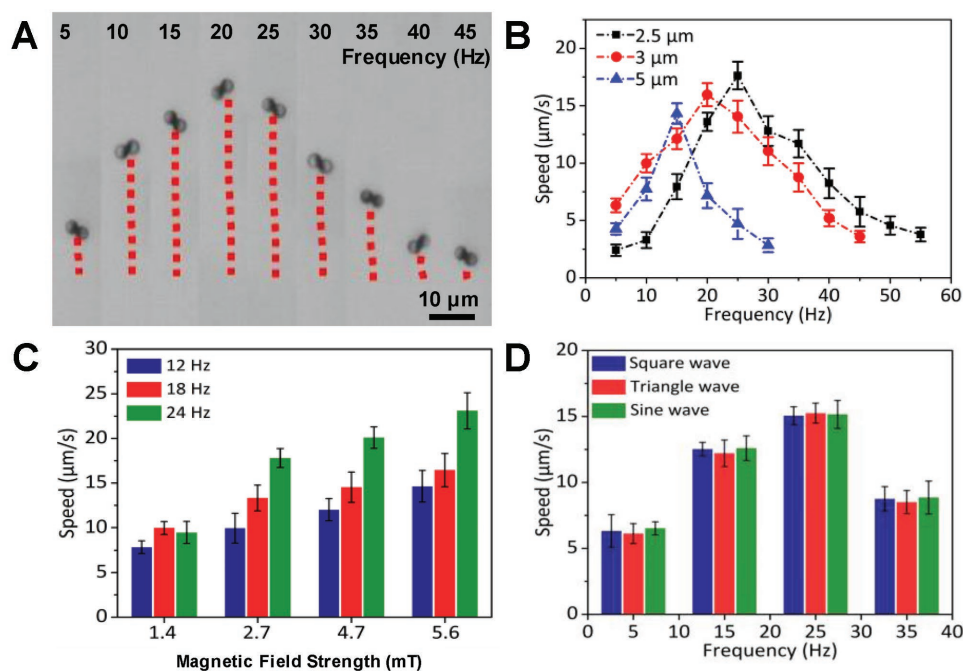


Figure 4. Performance of the microdimer surface walkers under different experimental parameters. A) Tracking lines illustrating the traveled distances of a microdimer surface walker over a 5 s period in an oscillating magnetic field with frequencies from 5 to 45 Hz. B) Speeds of the microdimer surface walkers with diameters of 2.5, 3, and 5 μm in a frequency range of 5–55 Hz. C) Speeds of the microdimer surface walkers at different magnetic field strength with driving frequencies of 12, 18, and 24 Hz. D) Speeds of the microdimer surface walkers at different driving frequencies of square, triangle, and sine waves.

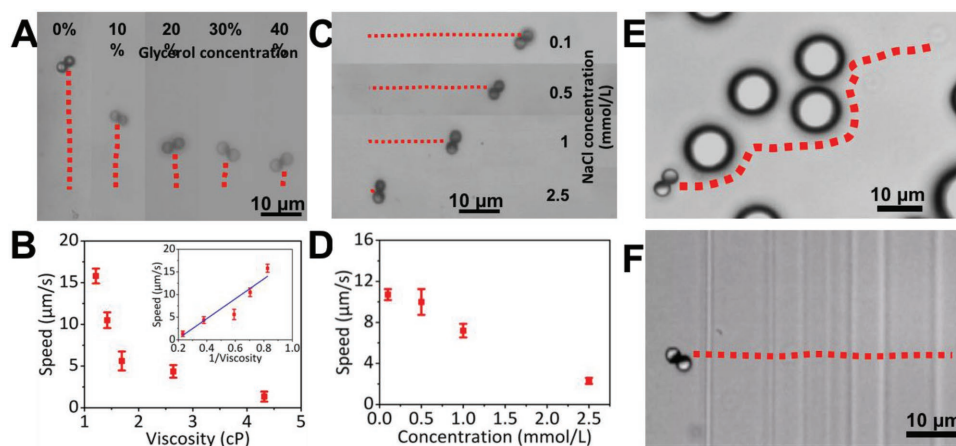


Figure 5. Performance of the microdimer surface walkers in complicated environments. Tracking lines illustrating the distance traveled by a microdimer surface walker over a 3 s period in aqueous solutions with different concentrations of A) glycerol and C) sodium chloride. B,D) Data for the experiments in (A) and (C). E) A microdimer surface walker bypasses several polystyrene microspheres 10 μm in diameter. F) A microdimer surface walker crosses continuous cracks on a glass surface.

The microdimers were then tested in sodium chloride solutions with various salt concentrations. Figure 5C displays the track lines of a microdimer over a 5 s period in these solutions. The velocity of the microdimer decreased from 10.7 to $2.3 \mu\text{m s}^{-1}$ upon increasing the sodium chloride concentration from 0.1 to 2.5 mmol L^{-1} (Figure 5D). Such a dramatic decrease in speed was somewhat surprising since in principle, magnetic fields are not significantly affected by the salt concentration of a solution beyond a small possible change in the magnetic susceptibility of the solution. We instead propose the following mechanism. As the salt concentration increases, it screens the charges on both the particles and the substrate, thus undermining the electrostatic repulsion from their electrical double layers. The dimers therefore settle closer to the bottom of the solution. We estimated that the separation distance changed from $1.36 \mu\text{m}$ to 64.2 nm upon increasing the salt concentration from 0 to 2.5 mmol L^{-1} (see the Supporting Information for the calculation details). The dimer dynamics strongly depend on its location near the bottom, and a smaller separation could mean more severe viscous drag for the spheres rolling both forward and backward, consequently slowing the dimer motion. Further increasing the salt concentration leads to an irreversible collapse in the electrical double layers and adhesion of the dimers to the bottom.

The ability to overcome/bypass complicated barriers is an extremely attractive feature of micromachines in applications ranging from nanomanipulation to precise medical treatments. Here, we demonstrate how the current magnetic microdimers circumvent small objects and overcome cracks along their paths. First, Figure 5E shows how a microdimer autonomously detoured around a 3D object comparable to its size ($10 \mu\text{m}$ microsphere) and continued along its original direction after the encounter. Figure 5F shows how a microdimer moved across continuous cracks created by scratching the glass slide with a diamond cutter. These examples (Video S4, Supporting Information) are only preliminary demonstrations but provide evidence for the robustness and power of these magnetic microdimers, which could prove valuable for future applications.

On-demand speed modulation and directional steering of microswimmers are also important features for many practical applications.^[10,13] Figure 6A presents the speed modulation of a microdimer surface walker. The track line represents the trajectory of a microdimer operated with an oscillating frequency that was repeatedly switched between 8 and 18 Hz . The instantaneous speed of the microdimer was tracked and is plotted in the inset, revealing a periodic change between two speeds that matches the switching frequency. The nickel coating on our dimer enables the magnetic steering of its motion, and Figure 6B,C presents the magnetic control of the directionality of the microdimer surface walkers. Since the dimer always aligns with the magnetic fields to minimize energy, a change in the relative position between the electromagnet and the surface walker in the x - y plane leads to a change in the motor orientation and moving direction (Figure 6B). Because the dimer is very sensitive to the direction of the magnetic field and responds precisely and quickly, complex trajectories such as that demonstrated in Figure 6C become possible (Video S5, Supporting Information). It is easy to imagine that more sophisticated magnetic setups involving multiple coils could lead to more advanced control over the dimer trajectory.

3. Conclusions

In conclusion, we have reported the propulsion and steering of magnetic microdimers in an oscillating magnetic field operated at $\approx 10 \text{ Hz}$. The two Ni-dielectric Janus spheres in the dimer rolled alternately and asymmetrically, and a peak speed of $\approx 20 \mu\text{m s}^{-1}$ was achieved at a field strength of $\approx 2.7 \text{ mT}$. The speed was significantly reduced in solutions with high viscosity or a high salt concentration, while modulation of the speed was easily achieved by ramping the driving voltage/frequency up and down. Due to the alignment of the microdimer with the magnetic field, fast and precise steering provided good control of the dimer trajectory and the ability to overcome obstacles. Regarding the operation mechanism, we tentatively proposed

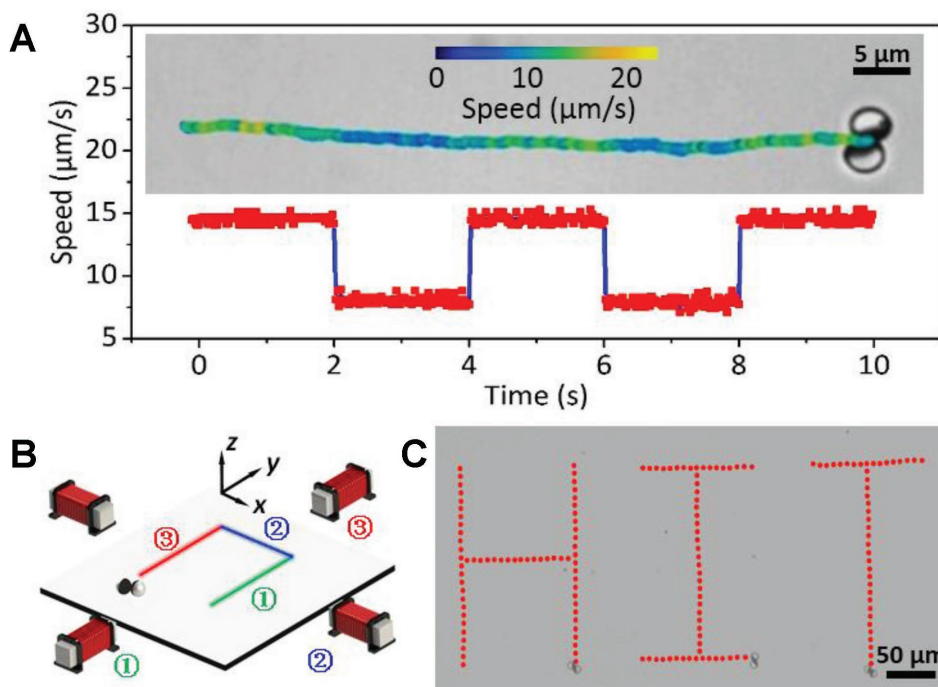


Figure 6. On-demand speed modulation and steering of microdimer surface walkers: A) Speed modulation of the surface walkers in response to a series of frequency ramp switches between 8 and 18 Hz. Inset: the trajectory of a dimer operated under switching frequencies in which the speed is color-coded. B) Scheme of the magnetic control of the microdimer surface walkers. By placing the magnets at different positions marked by 1, 2, and 3, the microdimer moves along different paths that are aligned with the respective magnet positions. C) Microdimer surface walkers are steered along specific paths that form the letters HIT.

that oscillating magnetic fields below the coercivity exerted torques that rolled the spheres, and their rolling became asymmetric due to the coupling of the field to the nearby boundaries and the presence of a field gradient. This rolling led to a net displacement that was not observed for microdimers levitated in the bulk solution in acoustic levitation experiments. The dynamics of the microdimers in which the two spheres alternate and walk on a surface carry an interesting, although superficial, similarity to protein nanomotors, such as kinesin and myosin, that walk on microtubular tracks, which obviously operate by a completely different mechanism and on a different scale. Overall, the microdimer surface walkers reported here are a new type of magnetic microswimmers, and, due to their easy operation and precise steering capabilities, could become a promising candidate for future applications in areas such as biomedicine and environmental monitoring.

4. Experimental Section

Synthesis of Janus Microspheres: Silica or polystyrene microsphere monolayers were produced on glass slides and coated with a 20 nm titanium layer at 1 \AA s^{-1} followed by a nickel layer of a desired thickness at 2 \AA s^{-1} using a Temescal BJD 1800 E-beam evaporator. Through brief sonication in ultrapure water, the Janus microspheres were released from the glass slide and dispersed in ultrapure water.

Magnetic Experiments: The magnetic field setup was adapted from previous studies,^[42,44,64] and consisted of a dual-channel arbitrary waveform generator (Keysight 33510B), a compact 150 W audio amplifier (SMSL, SA-S3), and a 10 mH iron core inductor (Erse Audio,

266-580). In a typical experiment, the magnet was placed a few cm from the experimental chamber, which was either a glass capillary tube or a chamber created by a silicone spacer, a glass substrate, and a cover slip. The tip of the iron core was pointed toward the chamber. The magnetic field strength at the center of the chamber dropped as the magnet was moved away from it, and this change was measured and is reported in Figure S1 (Supporting Information).

Optical Observation and Tracking: Videos were captured at 30 frames s^{-1} by an inverted optical microscope (Olympus IX73) coupled with a $40\times$ objective and a Point Grey CMOS camera. These videos were then analyzed by MATLAB codes courtesy of Prof. Hepeng Zhang from Shanghai Jiaotong University. The particles were isolated by the code, and their coordinates in each frame were identified. The trajectories and speeds of the particles were then obtained.

Ultrasound Experiments: The ultrasound experiments followed a procedure developed in a previous study.^[28] Briefly, ultrasound waves were produced by a piezoelectric transducer coupled to the back side of a piece of silicon wafer, and the experimental chamber sat on the front side of the wafer. The transducer was connected to one output channel of the dual-channel waveform generator (the other channel was connected to the magnetic setup), and sine waves of 3–4 MHz frequency were typically used. At the resonance frequency of the chamber, the particles were levitated by the acoustic radiation force to a nodal plane at the center of the chamber. The ultrasound was then turned off to allow the particles to settle, and their dynamics during settling were recorded.

Supporting Information

Supporting Information is available from the Wiley Online Library or from the author.

Acknowledgements

T.L. and A.Z. contributed equally to this work. The authors are grateful to Prof. Hepeng Zhang for helpful discussions. This project was financially supported by the National Natural Science Foundation of China (51705108, 91648201, 51521003, 11402069, and 11774075), the Key Laboratory of Micro-systems and Micro-structures Manufacturing of Ministry of Education (2016KM004), the Self-Planned Task of State Key Laboratory of Robotics and System (HIT) (SKLRS 201706A), the National Science and Technology Major Project (2016ZX05010-006), the Natural Science Foundation of Guangdong Province (No. 2107B030306005), and the Science Technology and Innovation Program of Shenzhen (JCYJ20170307150031119). T.L. is also supported by the General Financial Grant from the China Postdoctoral Science Foundation (2017M621257), and the General Financial Grant from the Heilongjiang Postdoctoral Science Foundation.

Conflict of Interest

The authors declare no conflict of interest.

Keywords

AC magnetic fields, Janus microspheres, kinetic optimization, magnetic actuation, micromotors

Received: October 19, 2017
Revised: November 27, 2017
Published online:

- [1] J. Wang, *Nanomachines: Fundamentals and Applications*, Wiley-VCH, Weinheim, Germany **2013**.
- [2] J. Li, B. Esteban-Fernández de Ávila, W. Gao, L. Zhang, J. Wang, *Sci. Rob.* **2017**, *2*, eaam6431.
- [3] B. J. Nelson, I. K. Kaliakatsos, J. J. Abbott, *Annu. Rev. Biomed. Eng.* **2010**, *12*, 55.
- [4] Y. Mei, A. A. Solovev, S. Sanchez, O. G. Schmidt, *Chem. Soc. Rev.* **2011**, *40*, 2109.
- [5] M. Guix, C. C. Mayorga-Martinez, A. Merkoci, *Chem. Rev.* **2014**, *114*, 6285.
- [6] H. Wang, M. Pumera, *Chem. Rev.* **2015**, *115*, 8704.
- [7] S. Sanchez, L. Soler, J. Katuri, *Angew. Chem., Int. Ed.* **2015**, *54*, 1414.
- [8] T. E. Mallouk, A. Sen, *Sci. Am.* **2009**, *300*, 72.
- [9] K. Kim, J. Guo, X. Xu, D. L. Fan, *Small* **2015**, *11*, 4037.
- [10] Z. Wu, X. Lin, T. Si, Q. He, *Small* **2016**, *12*, 3080.
- [11] F. Peng, Y. Tu, D. A. Wilson, *Chem. Soc. Rev.* **2017**, *46*, 5289.
- [12] B. Dai, J. Wang, Z. Xiong, X. Zhan, W. Dai, C. C. Li, S. P. Feng, J. Tang, *Nat. Nanotechnol.* **2016**, *11*, 1087.
- [13] L. Xu, F. Mou, H. Gong, M. Luo, J. Guan, *Chem. Soc. Rev.* **2017**, *46*, 6905.
- [14] T. Xu, W. Gao, L. P. Xu, X. Zhang, S. Wang, *Adv. Mater.* **2017**, *29*, 1603250.
- [15] J. G. Gibbs, S. Kothari, D. Saintillan, Y. Zhao, *Nano Lett.* **2011**, *11*, 2543.
- [16] J. Li, P. Angsantikul, W. Liu, B. Esteban-Fernández de Ávila, S. Thamphiwatana, M. Xu, E. Sandraz, X. Wang, J. Delezuk, W. Gao, L. Zhang, J. Wang, *Angew. Chem., Int. Edit.* **2017**, *56*, 2156.
- [17] X. Ma, K. Hahn, S. Sanchez, *J. Am. Chem. Soc.* **2015**, *137*, 4976.
- [18] W. Wang, S. Li, L. Mair, S. Ahmed, T. Huang, T. E. Mallouk, *Angew. Chem., Int. Ed.* **2014**, *53*, 3201.
- [19] T. Li, X. Chang, Z. Wu, J. Li, G. Shao, X. Deng, J. Qiu, B. Guo, G. Zhang, Q. He, L. Li, J. Wang, *ACS Nano* **2017**, *11*, 9268.
- [20] X. Ma, X. Wang, K. Hahn, S. Sanchez, *ACS Nano* **2016**, *10*, 3597.
- [21] R. Dong, J. Li, I. Rozen, B. Ezhilan, T. Xu, C. Christianson, W. Gao, D. Saintillan, B. Ren, J. Wang, *Sci. Rep.* **2015**, *5*, 13226.
- [22] J. Li, V. Singh, S. Sattayasamitsathit, J. Orozco, K. Kaufmann, R. Dong, W. Gao, B. Jurado-Sanchez, Y. Fedorak, J. Wang, *ACS Nano* **2014**, *8*, 11118.
- [23] T. Li, L. Li, W. Song, L. Wang, G. Shao, G. Zhang, *ECS J. Solid State Sci.* **2015**, *4*, S3016.
- [24] W. Gao, X. Feng, A. Pei, Y. Gu, J. Li, J. Wang, *Nanoscale* **2013**, *5*, 4696.
- [25] J. Palacci, S. Sacanna, A. P. Steinberg, D. J. Pine, P. M. Chaikin, *Science* **2013**, *339*, 936.
- [26] W. Wang, W. Duan, Z. Zhang, W. Sun, A. Sen, T. E. Mallouk, *Chem. Commun.* **2015**, *51*, 1020.
- [27] T. Xu, F. Soto, W. Gao, R. Dong, V. Garcia-Gradilla, E. Magana, X. Zhang, J. Wang, *J. Am. Chem. Soc.* **2015**, *137*, 2163.
- [28] W. Wang, L. A. Castro, M. Hoyos, T. E. Mallouk, *ACS Nano* **2012**, *6*, 6122.
- [29] J. Li, W. Liu, T. Li, I. Rozen, J. Zhao, B. Bahari, B. Kante, J. Wang, *Nano Lett.* **2016**, *16*, 6604.
- [30] J. Li, W. Gao, R. Dong, A. Pei, S. Sattayasamitsathit, J. Wang, *Nat. Commun.* **2014**, *5*, 5026.
- [31] W. Gao, X. Feng, A. Pei, C. R. Kane, R. Tam, C. Hennessy, J. Wang, *Nano Lett.* **2014**, *14*, 305.
- [32] A. Ghosh, P. Fischer, *Nano Lett.* **2009**, *9*, 2243.
- [33] D. Walker, B. T. Käschorf, H. H. Jeong, O. Lieleg, P. Fischer, *Sci. Adv.* **2015**, *1*, e1500501.
- [34] D. Schamel, A. G. Mark, J. G. Gibbs, C. Miksch, K. I. Morozov, A. M. Leshansky, P. Fischer, *ACS Nano* **2014**, *8*, 8794.
- [35] J. Li, S. Sattayasamitsathit, R. Dong, W. Gao, R. Tam, X. Feng, S. Ai, J. Wang, *Nanoscale* **2014**, *6*, 9415.
- [36] S. Tottori, L. Zhang, F. Qiu, K. K. Krawczyk, A. Franco-Obregon, B. J. Nelson, *Adv. Funct. Mater.* **2012**, *24*, 811.
- [37] L. Zhang, T. Petit, Y. Lu, B. E. Kratochvil, K. E. Peyer, R. Pei, J. Lou, B. J. Nelson, *ACS Nano* **2010**, *4*, 6228.
- [38] T. Yang, T. O. Tasci, K. B. Neeves, N. Wu, D. W. M. Marr, *Langmuir* **2017**, *33*, 5932.
- [39] J. Li, T. Li, T. Xu, M. Kiristi, W. Liu, Z. Wu, J. Wang, *Nano Lett.* **2015**, *15*, 4814.
- [40] R. Dreyfus, J. Baudry, M. L. Roper, M. Fermigier, H. A. Stone, J. Bibette, *Nature* **2005**, *437*, 862.
- [41] T. Qiu, T. C. Lee, A. G. Mark, K. I. Morozov, R. Munster, O. Mierka, S. Turek, A. M. Leshansky, P. Fischer, *Nat. Commun.* **2014**, *5*, 5119.
- [42] T. Li, J. Li, H. Zhang, X. Chang, W. Song, Y. Hu, G. Shao, E. Sandraz, G. Zhang, L. Li, J. Wang, *Small* **2016**, *12*, 6098.
- [43] B. Jang, E. Gutman, N. Stucki, B. F. Seitz, P. D. Wendel-Garcia, T. Newton, J. Pokki, O. Ergeneman, S. Pane, Y. Or, B. J. Nelson, *Nano Lett.* **2015**, *15*, 4829.
- [44] T. Li, J. Li, K. I. Morozov, Z. Wu, T. Xu, I. Rozen, A. M. Leshansky, L. Li, J. Wang, *Nano Lett.* **2017**, *17*, 5092.
- [45] P. Tierno, R. Golestanian, I. Pagonabarraga, F. Sagués, *Phys. Rev. Lett.* **2008**, *101*, 218304.
- [46] Z. Ye, M. Sitti, *Lab Chip* **2014**, *14*, 2177.
- [47] X. Chen, N. Shamsudhin, M. Hoop, R. Pieters, E. Siringil, M. S. Sakar, B. J. Nelson, S. Pane, *Mater. Horiz.* **2016**, *3*, 113.
- [48] T. O. Tasci, P. S. Herson, K. B. Neeves, D. W. M. Marr, *Nat. Commun.* **2016**, *7*, 10225.
- [49] C. E. Sing, T. C. Lubensky, *Proc. Natl. Acad. Sci. USA* **2010**, *107*, 535.
- [50] T. Petit, L. Zhang, K. E. Peyer, B. E. Kratochvil, B. J. Nelson, *Nano Lett.* **2012**, *12*, 156.
- [51] S. Kim, F. Qiu, S. Kim, A. Ghanbari, C. Moon, L. Zhang, B. J. Nelson, H. Choi, *Adv. Mater.* **2013**, *25*, 5863.
- [52] C. Bechinger, R. D. Leonardo, H. Löwen, C. Reichhardt, G. Volpe, G. Volpe, *Rev. Mod. Phys.* **2016**, *88*, 045006.

- [53] A. E. Patteson, A. Gopinath, P. E. Arratia, *Curr. Opin. Colloid Interface Sci.* **2016**, *21*, 86.
- [54] C. Liu, C. Zhou, W. Wang, H. P. Zhang, *Phys. Rev. Lett.* **2016**, *117*, 198001.
- [55] J. Simmchen, J. Katuri, W. E. Uspal, M. N. Popescu, M. Tasinkevych, S. Sánchez, *Nat. Commun.* **2016**, *7*, 10598.
- [56] B. Ren, A. Ruditskiy, J. H. Song, I. Kretzschmar, *Langmuir* **2012**, *28*, 1149.
- [57] S. Gangwal, A. Pawar, I. Kretzschmar, O. D. Velev, *Soft Matter* **2010**, *6*, 1413.
- [58] S. K. Smoukov, S. Gangwal, M. Marquez, O. D. Velev, *Soft Matter* **2009**, *5*, 1285.
- [59] E. L. Jewell, W. Wang, T. E. Mallouk, *Soft Matter* **2016**, *12*, 2501.
- [60] W. Wang, W. Duan, A. Sen, T. E. Mallouk, *Proc. Natl. Acad. Sci. USA* **2013**, *110*, 17744.
- [61] M. S. D. Wykes, J. Palacci, T. Adachi, L. Ristorph, X. Zhong, M. D. Ward, J. Zhangade, M. J. Shelleya, *Soft Matter* **2015**, *12*, 4584.
- [62] J. Yan, M. Bloom, S. C. Bae, E. Luijten, S. Granick, *Nature* **2012**, *491*, 578.
- [63] S. Q. Choi, S. G. Jang, A. J. Pascall, M. D. Dimitriou, T. Kang, C. J. Hawker, T. M. Squires, *Adv. Mater.* **2011**, *23*, 2348.
- [64] P. Kinnunen, B. H. Mcnaughton, J. Niinimaki, *Rev. Sci. Instrum.* **2013**, *84*, 086109.